Optical properties and electronic structure of the Cu-Zn brasses

V. J. Keast[1], J. Ewald[1], K.S.B. De Silva[2], M. B. Cortie[2], B. Monnier[3,4], D. Cuskelly[3] and E. H. Kisi[3]

[1]School of Mathematical and Physical Sciences, The University of Newcastle, Callaghan NSW 2308, Australia

[2]Institute for Nanoscale Technology, University of Technology Sydney, PO Box 123, Broadway, NSW 2007, Australia

[3]School of Engineering, The University of Newcastle, Callaghan NSW 2308, Australia

[4]on attachment from Universite de Technologie de Troyes,12 rue Marie Curie, BP 2060, 10010 Troyes cedex France/

Abstract

The color of Cu-Zn brasses range from the red of copper through to bright yellow to grey-silver as the Zn content increases and they have a wide range of decorative and technical applications. The optical properties of this set of alloys has been calculated using density functional theory (DFT) and compared to experimental spectroscopy measurements. The optical response of the low Zn content α-brasses is shown to have a distinctly different origin to that in the higher content β', γ and ε-brasses. The response of β'-brass is unique in that it is strongly influenced by an overdamped plasmon excitation and this alloy will also have a strong surface plasmon response.

PACS number(s): 71.20.Be, 78.20.Bh, 81.05.Bx

I. INTRODUCTION

The unique optical properties of the noble (or coinage) metals, Cu, Ag, Au and their alloys, have been applied for centuries in a variety of technological and decorative purposes. Most recently they have been the predominant materials used for plasmonic applications. It has been demonstrated that nanoparticles can be fabricated from Cu-Zn alloys [1-6] and that a surface plasmon resonance can be sustained [3, 6]. The color of the bulk Cu-Zn brasses varies with the Zn content, as does the energy of the plasmon resonance in nanoparticles. This behavior is related to the change in the dielectric function that occurs with the different composition and crystal structure of the alloys. The dielectric function is itself determined by the underlying electronic structure of the material.

A number of Cu-Zn alloys and intermetallic phases are observed, as listed in Table I. Inclusion of vacancies in the structures allows these phases to span a finite composition range in the binary phase diagram. The Cu-Zn system has long been studied as the prototypical representative of materials satisfying the Hume-Rothery rules [7]. Despite this long history, there is an incomplete understanding of the connections between the crystal structure, electronic structure and optical properties in these materials.

The α-brass phase occurs when the Zn content is below about 30 at.% and it has a disordered, substitutional, face centred cubic (fcc) structure. As the Zn content increases the color transforms from the reddish hue of pure Cu to the bright yellow of brass. Associated with this color change, the optical absorption edges shift upwards in energy as the Zn content increases [8-11]. The α-brasses have also been the subject of many theoretical investigations where it has been concluded that the alloying with Zn shifts the valence band features down in energy [12-15]. This is consistent with the increase in the energy of interband transitions that are responsible for the absorption edge [12]. The correlation between the various features in the optical spectra with transitions from the bandstructure was made by Rao et al. [16]. The onset of these interband transitions is usually

identified as being from the top of the *d*-band, but the origin of the features at higher energy has been the subject of some debate.

For the equiatomic composition and at high temperatures (above 480ºC), β-brass (CuZn) is disordered body centred cubic (bcc) but this structure is not retained when the alloy is quenched and the β'-brass usually has the CsCl structure. The color and reflectivity changes in β'-brass (along with other alloys) was measured as a function of temperature below the disorder transition by Muldawer [17]. An analogy was drawn between it and Ag, as both metals display a sharp reflectivity dip, which is in contrast to Au and pure Cu. It was proposed that bulk plasmon excitations play an important role in accounting for this behaviour. The Muldawer data was later used to extract the dielectric functions for β'-brass which showed that the real part of the dielectric function, ε_1, crosses zero at ~2.5 eV, which is where the reflectivity dip occurs [18]. However, it was necessary to perform extrapolation of the data, including matching to pure Cu data outside the measured frequency range, in order to perform the Kramers-Kronig analysis. Later measurements have instead suggested that, although ε_1 closely approaches zero at the energy of the reflectivity dip, it does not actually cross the axis [19].

There have been a number of calculations of the electronic structure and bandstructure of β'-brass [14, 20-22] and there were discrepancies in the energy position of the *d*-band between the early results. The main peak in the complex part of the dielectric function, ε_2, has been attributed to transitions from the Fermi surface to the unoccupied states [20, 21, 23] but it has also been suggested that transitions from the *d*-band also contribute [24]. Although the earlier papers discussed the important role of the bulk plasmon in the color and optical response of β'-brass [17, 18], this aspect has largely been neglected in later papers [23]. Indeed, the question of whether ε_1 for β'-brass crosses zero at 2.5 eV, corresponding to the energy at which a bulk plasmon excitation would occur, does not appear to have been resolved.

The electronic structure of γ-brass has previously been studied in order to understand the phase stability of this complex metal alloy [25, 26] but the optical properties have remained largely unexplored, apart from a recent experimental study of thin film samples [27]. We are not aware of any studies of the electronic structure and optical properties of ε-brass. These Zn rich γ and ε phases do not display the golden hues of the brasses with low Zn content.

This paper calculates the electronic structure of the α-, β'-, γ- and ε-Cu-Zn brasses using density functional theory (DFT). Two compositions (12.5 and 25 at.% Zn) were calculated for the α-phase. From the electronic structure, the dielectric function and reflectivity were calculated using the random phase approximation (RPA). The calculations are compared to optical data acquired from thin film and bulk samples. In previous work on the α- and- β-phases, the connection between the electronic structure and the optical response was only inferred, not calculated. The calculations presented here represent the first direct calculation of the optical responses. For the other alloys this work represents the first computational study of their optical responses. By comprehensively studying the set of alloys, the trends and differences between the different Cu-Zn brasses were explored and the origin of this behaviour was established.

II. EXPERIMENTAL DETAILS

Thin film samples were prepared by co-depositing the elements on onto a glass substrate by direct current magnetron sputtering. Substrate surfaces were thoroughly cleaned using detergent, water, acetone and ethanol then dried in nitrogen. The base pressure of the chamber was 1.3×10^{-4} Pa (~ 10^{-6} Torr) with flow of argon at a pressure of 0.2 Pa (1.5 mTorr).

Bulk samples were prepared by induction melting 99.99% pure Cu and Zn within a carbon crucible under a flowing argon atmosphere. The resulting ~24 mm diameter, ~50 mm long ingot samples were then sectioned using a diamond saw, ground and lapped to a 1μm diamond polish.

Crystal structures were verified using Cu K_α X-Ray Diffraction (XRD) on a Panalyitical ExPert™ diffractometer or a Siemens D5000 X-ray diffractometer. The sample compositions were measured with energy dispersive spectra using a Zeiss Evo LS15 SEM with a Bruker EDS Quantax 400. Prior to optical characterisation the bulk samples were subjected to find grinding and polishing operations, where 0.05 μm gamma-alumina suspension was used at the final polishing. Optical characterization was carried out using a V-VASE Ellipsometer by J.A. Woollam Co.. The resultant data was analyzed using WVASE ellipsometric software.

Samples for transmission electron microscopy (TEM) were prepared from the bulk alloys by the conventional approaches of mechanical polishing, dimple grinding and ion beam thinning. TEM images and diffraction patterns were acquired using a JEOL 2100 LaB_6 TEM.

III. COMPUTATIONAL METHODS

The experimental crystal structures for the β'- and γ-phases, as given in Table I, were used in the DFT calculations. The disordered structures of α-$Cu_{0.875}Zn_{0.125}$, α-$Cu_{0.75}Zn_{0.25}$ and ε-$Cu_{0.20}Zn_{0.80}$ cannot be modelled with the methods used here and so, for these, a supercell and specific atom sites were chosen as shown in Fig. 1. Experimental lattice parameters from the literature for the two different compositions of the α-phases were used [28]. For the ε-phase, 3 of the 16 atoms in a 2x2x2 supercell were set to Cu which corresponds to a Zn concentration of 81.25 at.% and the experimental lattice parameters from the literature for an 81.5 at.% alloy were used [29]. For the α-$Cu_{0.75}Zn_{0.25}$ alloy, a selection of three structures were modelled and compared in order to test the effect of atom positions on the optical responses. These have been designated A, B and C for reference as indicated in Fig. 1.

The DFT calculations were performed using the (linearized) augmented plane wave plus local orbitals method (LAPW+lo) within the WIEN2K software package [30]. This is an all-electron method that includes relativistic effects. The generalized gradient approximation (GGA) of Perdew,

Burke, and Ernzerhof (PBE) was used for the exchange-correlation potential [31]. The number of *k*-points was set sufficiently high that the resultant spectral details are not expected to change with more *k*-points. The maximum angular momentum for the radial wave functions (l_{max}) was chosen as 10 and the plane-wave cut-off ($R_{MT}K_{max}$) was set to 7.0.

The total and partial density of states (DOS) were calculated by means of the modified tetrahedron method [32]. The complex dielectric function was calculated using the random phase approximation (RPA) and neglecting local field effects (LFE) [33]. The RPA approximates the polarizability of the system as a sum over independent transitions. The momentum matrix elements are calculated from the electron states and an integration over the irreducible Brillioun zone is performed to calculate $\varepsilon_2(\omega)$. Finally, a Kramers–Kronig analysis is performed to obtain $\varepsilon_1(\omega)$. LFE are not expected to be significant in the low-energy spectral regions of interest here [34]. It is computationally convenient to split the calculations of the dielectric function due to inter- and intraband transitions into two separate calculations before summing them to obtain the final dielectric function. For non-cubic systems, an appropriate average over the different components of the dielectric function (ε_{xx}, ε_{yy}, ε_{zz}) was performed. In order to elucidate the connection between the DOS and optical response functions, the response functions were also calculated with a subset of band-to-band contributions. Further details about the calculation of optical properties using WIEN2k can be found elsewhere [35].

IV. RESULTS

Table II. summarises the details of the composition and structure of the Cu-Zn samples fabricated in this work. The low boiling point of Zn makes it challenging to retain the Zn content during the fabrication of bulk samples.

Fig. 2 shows the calculated total DOS for each of the crystal structures (but only structure A for α-$Cu_{0.75}Zn_{0.25}$). Figs. 3 (a) and (b) show the real and imaginary parts of the calculated dielectric

functions and Figs. 3 (c) and (d) the corresponding experimental data. Fig. 4 shows the experimental and calculated reflectivity. Also shown in Fig. 2, with a dashed line, is the DOS for the electronic bands that a band analysis shows make the major contribution to the onset of the interband transitions for that alloy, as illustrated in Fig. 5. This analysis shows that for the α-brasses the absorption threshold is associated with transitions from the top of the *d*-band, as is the case with pure Cu. In contrast, for the β-, γ- and ε-brasses it is primarily the transitions from just below the Fermi level that contribute to the onset of the main peak in ε_2, with the *d*-band transitions making a much smaller contribution.

Fig. 6 shows the reflectivity calculated for the three different structures of α-$Cu_{0.75}Zn_{0.25}$. It indicates that the effect of structural rearrangements on the optical properties is generally smaller than the effect of a change in composition. It could be expected that a disordered alloy would show an optical response that is an average of such calculations.

Fig. 7 shows images and corresponding diffraction patterns for the bulk β-, γ- and ε-brasses. The β- and γ-brasses were large grained and indexing a low-index diffraction pattern as shown confirmed the crystal structures. The ε-brass was quite fine grained showing a more polycrystalline diffraction pattern. The first ring of spots corresponds to the [110] d-spacing for ε-brass. The TEM images of the β- and ε-brasses show many dislocations and other defects whereas the γ-brass is quite featureless and defect free.

V. DISCUSSION

For all alloys, the valence DOS is dominated by two distinct *d*-bands: the lower energy band corresponding to the Zn states; and the higher one to the Cu states. As expected, as the Zn content increases the Cu *d*-band becomes smaller and narrower and the Zn *d*-band correspondingly larger and wider. The top of the Cu *d*-band shows a slight shift downwards, relative to the Fermi level

with increasing Zn content. The DOS presented here are consistent with results in the literature, where available [14, 22, 24-26, 36].

As the Zn content in α-brass increases, the absorption edge shifts slightly upwards in energy, consistent with prior observations and calculations [12-16]. In the α-brasses, the color and absorption edge onset arise from transitions from the top of the *d*-band with only a small contribution from the states around the Fermi level. In contrast, for the β–, γ–, and ε-brasses, it is primarily the transitions around the Fermi level that contribute to the main peak in ε_2 with the *d*-band transitions making a much smaller contribution. There is not a monotonic relationship between the energy of the main peak and the Zn content for this group of alloys, with the γ-brass having the lowest energy and strongest interband transitions. The γ-brass has the most complex crystallographic structure, resulting in a complicated bandstructure with many available interband transitions, which accounts for this behavior.

Generally, the calculated and experimental results show good agreement in the observed trends as function of Zn content. The energies of the peaks in ε_2 (and corresponding dips in the reflectivity) are well reproduced, particularly for the β–, γ–, and ε-brasses. However, the shape of the dielectric function for ε-brass does not agree well. The fabricated alloy had a number voids, defects and second phases. It was relatively dull in appearance, indicating significant additional absorption mechanisms, and this accounts for this discrepancy between the theoretical and experimental results. Similarly, there is a difference between the thin film and bulk results for β-brass which is most likely due to the differences in microstructure with these different fabrication methods.

The calculated absorption edge onset for the α-brasses is ~0.5 eV below the experimental values. One of the ongoing challenges in the study of the noble metals is that the relative energies of the features in the electronic structure are not well reproduced by calculations using conventional ground state density functional theory (DFT). This is particularly problematic for the tightly bound

d-states. The inclusion of dynamic quasiparticle effects has been shown to overcome this limitation [37-40], but such approaches are computationally quite demanding. Notwithstanding this limitation, interpretation of the origin of various features in the spectrum and the trends with changes in composition can still be performed using less sophisticated approaches.

The calculations here confirm that the color shift from a reddish hue of pure Cu to the yellow color of the α-brasses is accounted for by the shift upwards in energy of the absorption onset, due to the deeper lying d-band. The colorless hue of the γ- and ε- brasses is attributed to the large number of low-energy interband transitions around the Fermi level, not involving the *d*-band for these alloys. Similarly, transitions from the *d*-band are not involved in the optical response and color of the β-brass, despite this alloy having a brilliant yellow color. In this case, the reflectivity shows a sharp dip and then increases again, indicative of a plasmonic response.

In this work, neither the calculations nor experimental results have ε_1 in β'-brass crossing zero at ~2.5 eV, although it approaches very close to the axis. For the computational results, the spectra are calculated over an extended energy range (0-50 eV) and so issues around extrapolation to perform the Kramers-Kronig analysis are not important. Variables such a broadening parameters and k-point convergence were tested, and although they did influence the proximity to the axis, the calculations do not predict a crossing. For the experimental measurements, the use of ellipsometry techniques overcomes the ambiguities due to spectral extrapolation that occurred in the earlier work [17].

The existence of a longitudinal bulk plasmon is usually defined as when ε_1 crosses zero with a positive slope. Correspondingly, in an electron energy-loss experiment a peak in the energy-loss spectrum would be observed at this energy. The situation in β'-brass can be thought of as analogous to an overdamped spring where here the oscillation is strongly damped by the interband transitions. Nevertheless, the shape of dielectric function for β'-brass, suggests is would support a surface plasmon response at around 2-2.5 eV, depending on the shape of the particle. In this energy range,

ε_2 is quite small (few interband transitions) and so quite a strong response would be expected and this has been observed experimentally [6]. While the addition of small amounts of Zn to form the a-brasses should improve the plasmonic response of Cu, even greater improvement would be expected for the equiatomic intermetallic compound. β'-CuZn.

VI. CONCLUSION

The trends in behaviour of the optical properties of the Cu-Zn brasses have been successfully predicted using DFT. The optical response of the α-brasses is shown to be dominated by transitions from the top of the *d*-band whereas for the β-, γ-, and ε-brasses it is transitions around the Fermi level that are important. In addition a strongly damped bulk plasmon response plays a role in the optical response of β-brass and this material is expected to be useful for applications relying on the excitation of surface plasmons.

ACKNOWLEDGEMENTS

This research was supported under Australian Research Council's Discovery Projects funding scheme (Project Number DP120102545).

REFERENCES

[1] R. E. Cable and R. E. Schaak, Chem. Mater. **19**, 4098 (2007).

[2] M. Farbod and A. Mohammadian, Intermetallics **45**, 1 (2014).

[3] J. Hambrock, M. K. Schöter, A. Birkner, C. Wöll, and R. A. Fischer, Chem. Mater. **15**, 4217 (2003).

[4] Z. L. Schaefer, D. D. Vaughn, and R. E. Schaak, Journal of Alloys and Compounds **490**, 98 (2010).

[5] K. Schütte, H. Meyer, C. Gemel, J. barhel, R. A. Fischer, and C. Janiak, Nanoscale **6**, 3116 (2014).

[6] N. Suzuki and S. Ito, J. Phys. Chem. B **110**, 2084 (2006).

[7] R. F. Berger, P. L. Walters, S. lee, and R. Hoffmann, Chemical Reviews **111**, 4522 (2011).

[8] M. A. Biondi and J. A. Rayne, Phys. Rev. **115**, 1522 (1959).

[9] R. E. Hummel, J. Alfaro Holbrook, and J. B. Andrews, Surface Science **37**, 717 (1973).

[10] R. E. Hummel and J. B. Andrews, Phys. Rev. B **8**, 2449 (1973).

[11] G. P. Pells and H. Montgomery, J. Phys. C: Metal Phys. Suppl. **3**, S330 (1970).

[12] H. Amar, K. H. Johnson, and C. B. Sommers, Phys. Rev. **153**, 655 (1967).

[13] A. Bansil, H. Ehrenreich, L. Schwartz, and R. E. Watson, Phys. Rev. B **9**, 445 (1974).

[14] R. S. Dhaka, S. Banik, A. K. Shukla, V. Vyas, A. Chakrabarti, S. R. Barman, B. L. Ahuja, and B. K. Sharma, Phys. Rev. B **78**, 073107 (2008).

[15] M. M. Pant and S. K. Joshi, Phys. Rev. **184**, 635 (1969).

[16] R. S. Rao, R. Prasad, and A. Bansil, Phys. Rev. B **28**, 5762 (1983).

[17] L. Muldawer, Phys. Rev. **127**, 1551 (1962).

[18] K. H. Johnson and R. J. Esposito, J. Opt. Soc. Am. **54**, 474 (1964).

[19] H. P. Myers and L. Lindner, Physica Scripta **12**, 253 (1975).

[20] F. J. Arlinghaus, Phys. Rev. **186**, 609 (1969).

[21] K. H. Johnson and H. Amar, Phys. Rev. **139**, 760 (1965).

[22] V. L. Moruzzi, A. R. Williams, J. F. Janak, and C. Sofes, Phys. Rev. B **9**, 3316 (1974).

[23] I. I. Sasovskaya and V. P. Korabel, Phys. stat. sol. (b) **14**, 621 (1986).

[24] H. L. Skriver and N. E. Christensen, Phys. Rev. B **8**, 3778 (1973).

[25] R. Asahi, H. Sato, T. Takeuchi, and U. Mizutani, Phys. Rev. B **71**, 165103 (2005).

[26] O. Gourdon, D. Gout, D. J. Williams, T. Proffen, S. Hobbs, and G. J. Mills, Inorganic Chemistry **46** (2007).

[27] G. Yang, J. Sun, and J. Zhou, J. Appl. Phys. **111**, 073103 (2012).

[28] R. H. Heidersbach and E. D. Verink, Corrosion-NACE **28**, 397 (1972).

[29] T. B. Massalski and H. W. King, Acta Metallurgica **10**, 1171 (1962).

[30] P. Blaha, K. Schwarz, G. K. H. Madsen, D. Kvasnicka, and J. Luitz., Technische Universitat Wien, Austria, 2001).

[31] J. P. Perdew, S. Burke, and M. Ernzerhof, Phys. Rev. Lett. **77**, 3865 (1996).

[32] P. E. Blöchl, O. Jepsen, and O. K. Andersen, Phys. Rev. B **49**, 16223 (1994).

[33] C. Ambrosch-Draxl and J. O. Sofo, Computer Physics Communications **175**, 1 (2006).

[34] N. Vast, L. Reining, V. Olevano, P. Schattschneider, and B. Jouffrey, Phys. Rev. Lett. **88**, 037601 (2002).

[35] V. J. Keast, Micron **44**, 93 (2013).

[36] D. A. Rowlands, J. B. Staunton, B. L. Gyorffy, E. Bruno, and B. Ginatempo, Phys. Rev. B **72**, 045101 (2005).

[37] A. Marini and R. Del Sole, Phys. Rev. Lett. **91**, 176402 (2003).

[38] A. Marini, R. Del Sole, and G. Onida, Phys. Rev. B **66**, 115101 (2002).

[39] A. Marini, G. Onida, and R. Del Sole, Phys. Rev. B **64**, 195125 (2001).

[40] A. Marini, G. Onida, and R. Del Sole, Phys. Rev. Lett. **88**, 016403 (2002).

[41] Inorganic Crystal Structure Database, www.fiz-karlsruhe.de.

TABLE I. Crystal structures of the Cu-Zn brasses (from the Inorganic Crystal Structure Database [41]).

	Space Group	Lattice Parameters (Å)	Atomic Coordinates				Wyckoff Site
				x	y	z	
Cu	Fm-3m	a = 3.615	Cu	0	0	0	4a
α-$Cu_{1-x}Zn_x$	Fm-3m	a = 3.62 - 3.69	Cu/Zn	0	0	0	4a
β'-CuZn	Pm-3m	a = 2.959	Cu	0	0	0	1a
			Zn	½	½	½	1b
γ-Cu_5Zn_8	I-43m	a = 8.878	Zn	0.1089	0.1089	0.1089	8c
			Cu	0.328	0.328	0.328	8c
			Cu	0.3558	0	0	12e
			Zn	0.3128	0.3128	0.0366	24g
ε-$Cu_{0.20}Zn_{0.80}$	$P6_3/mmc$	a = 2.7418 c = 4.2939	Cu/Zn	⅓	⅔	¼	2c

TABLE II. Measured composition and lattice parameters for the thin film and bulk materials prepared in this work.

Sample (Nominal Composition)	Measured Composition	Space Group, Lattice Parameters (Å)
α-$Cu_{0.875}Zn_{0.125}$ thin film	86 at% Cu, 14 at% Zn	Fm-3m, a = 3.6446
α-$Cu_{0.75}Zn_{0.25}$ thin film	76 at% Cu, 24 at% Zn	Fm-3m, a = 3.6718
β'-$Cu_{0.50}Zn_{0.50}$ thin film	52 at% Cu, 48 at% Zn	Pm-3m, a = 2.9330
β'-$Cu_{0.50}Zn_{0.50}$ bulk	59 at% Cu, 41 at% Zn	Pm-3m, a = 2.9554
γ-Cu_5Zn_8 bulk	38 at% Cu, 62 at% Zn	I-43m, a = 8.8621
ε-$Cu_{0.20}Zn_{0.80}$ bulk	23 at% Cu, 77 at% Zn	$P6_3/mmc$, a = 2.7414, c = 4.2949

FIGURE CAPTIONS

FIG. 1. The supercell-based crystal structures used to model the disordered ε- and α-Cu-Zn brasses.

FIG. 2. Total DOS for (a) α-$Cu_{0.875}Zn_{0.125}$ (b) α-$Cu_{0.75}Zn_{0.25}$ (c) β'-CuZn (d) γ-Cu_8Zn_5 (e) ε-Cu_3Zn_{16}. The dashed line is the DOS for the electronic bands that a band analysis shows make the major contribution to the onset of the interband transitions (as shown in Fig. 5.). The dashed vertical line indicates the Fermi energy.

FIG. 3. Real part (a) (c) and imaginary parts (b) (d) of the dielectric function (ε) for Cu-Zn alloys as obtained from (a) (b) DFT calculations and (c) (d) experimental ellipsometry measurement.

FIG. 4. Reflectivity for Cu-Zn alloys as obtained from (a) DFT calculations and (b) experimental ellipsometry measurement.

FIG. 5. Comparison of the imaginary part of the dielectric function (ε_2) calculated using all interband transitions (solid line) to that calculated using only the transitions from bands represented by the dashed line in the DOS of Fig. 2 (dashed line). Calculated for (a) α-$Cu_{0.875}Zn_{0.125}$ (b) α-$Cu_{0.75}Zn_{0.25}$ (c) β'-CuZn (d) γ-Cu_8Zn_5 (e) ε-Cu_3Zn_{16}.

FIG. 6. Reflectivity calculated for the three different structures (A, B and C from Fig. 1) of α-$Cu_{0.75}Zn_{0.25}$.

FIG. 7. TEM images and diffraction patterns from bulk samples of (a) β-brass (b) γ-brass and (c) ε-brass.

FIG 1

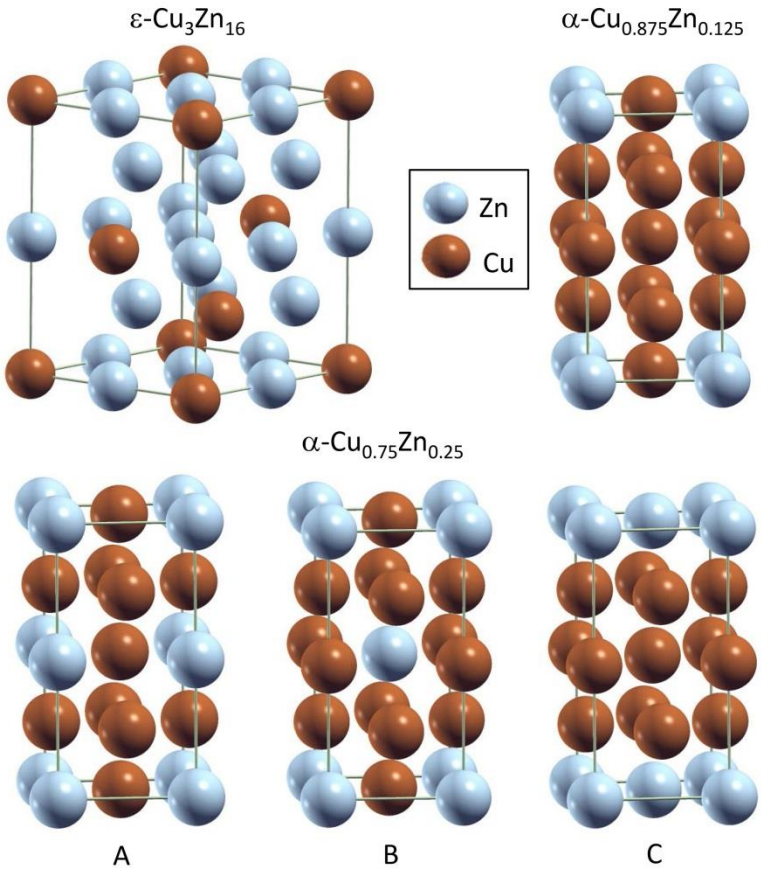

FIG 2

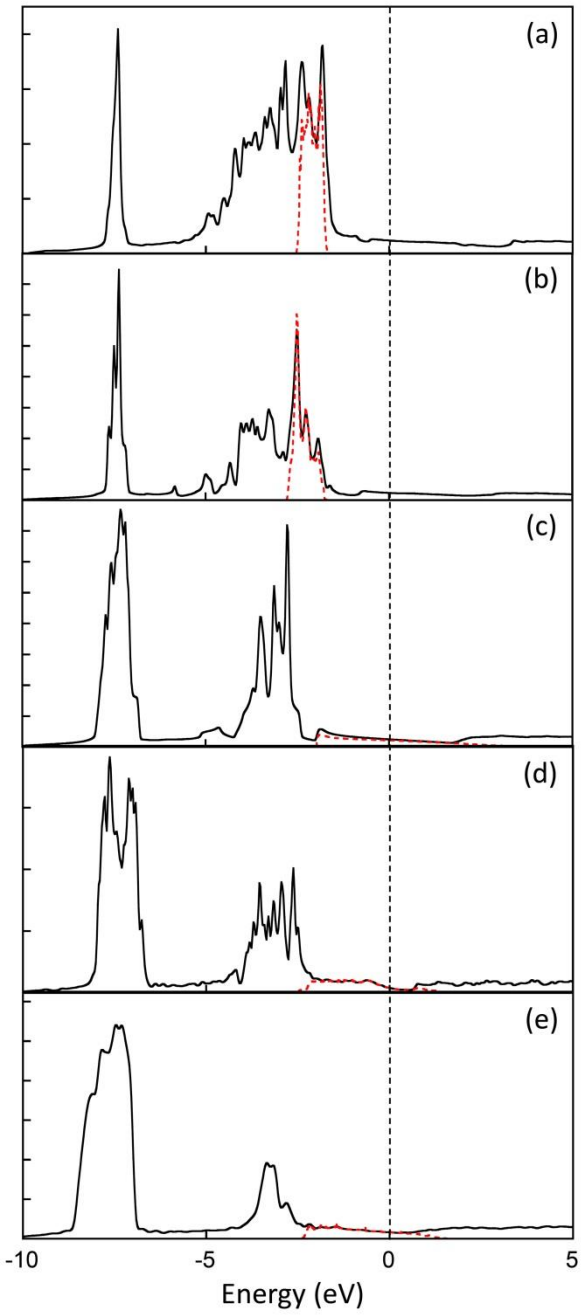

FIG 3

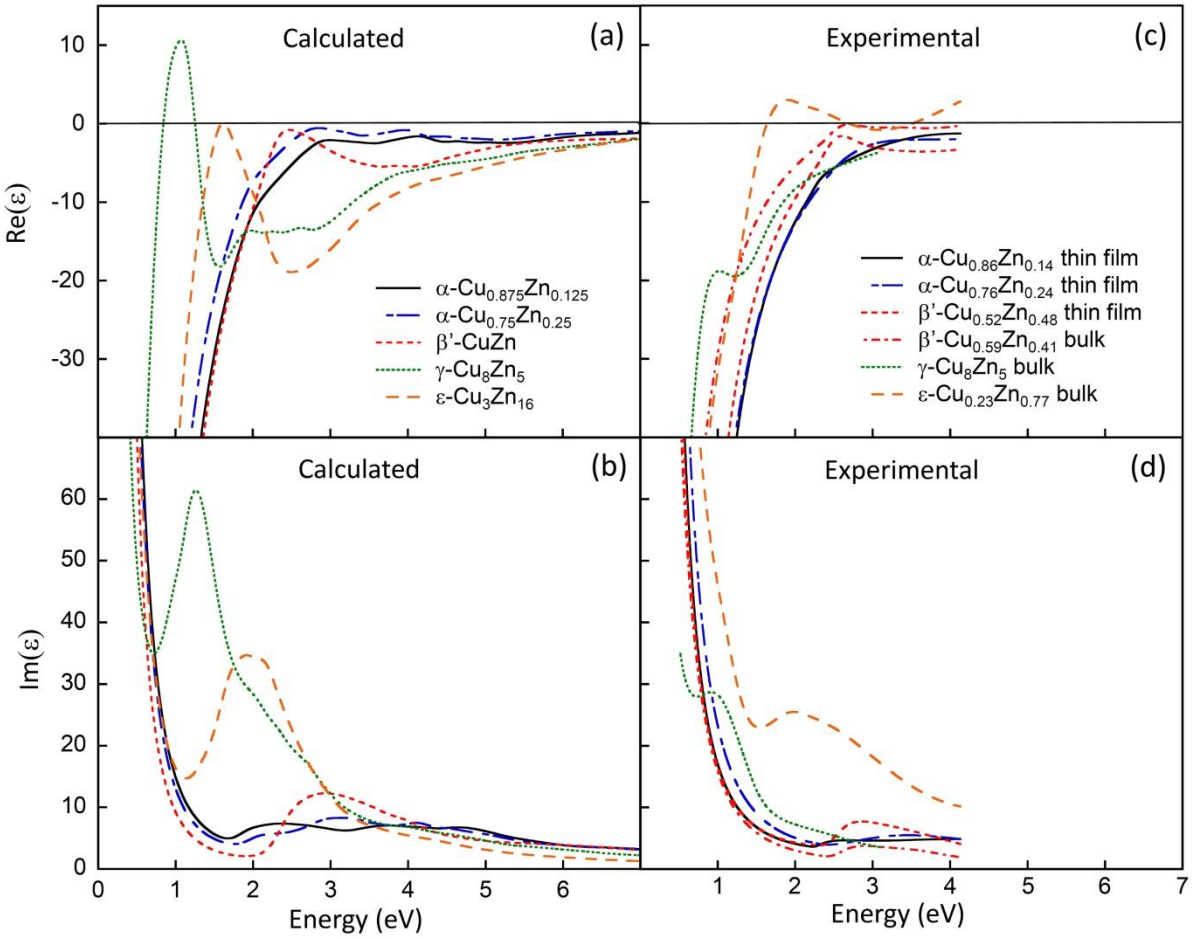
Calculated
(a)
Experimental
(c)
Re(ε)
α-Cu0.875Zn0.125
α-Cu0.75Zn0.25
β'-CuZn
γ-Cu8Zn5
ε-Cu3Zn16
α-Cu0.86Zn0.14 thin film
α-Cu0.76Zn0.24 thin film
β'-Cu0.52Zn0.48 thin film
β'-Cu0.59Zn0.41 bulk
γ-Cu8Zn5 bulk
ε-Cu0.23Zn0.77 bulk
Calculated
(b)
Experimental
(d)
Im(ε)
Energy (eV)
Energy (eV)

FIG 4

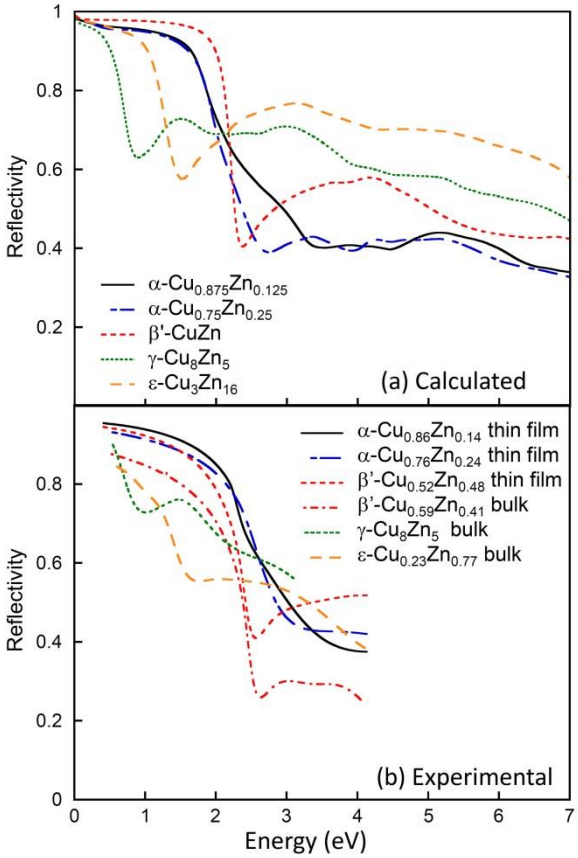
Reflectivity
α-Cu0.875Zn0.125
α-Cu0.75Zn0.25
β'-CuZn
γ-Cu8Zn5
ε-Cu3Zn16
(a) Calculated
α-Cu0.86Zn0.14 thin film
α-Cu0.76Zn0.24 thin film
β'-Cu0.52Zn0.48 thin film
β'-Cu0.59Zn0.41 bulk
γ-Cu8Zn5 bulk
ε-Cu0.23Zn0.77 bulk
(b) Experimental
Energy (eV)

FIG 5

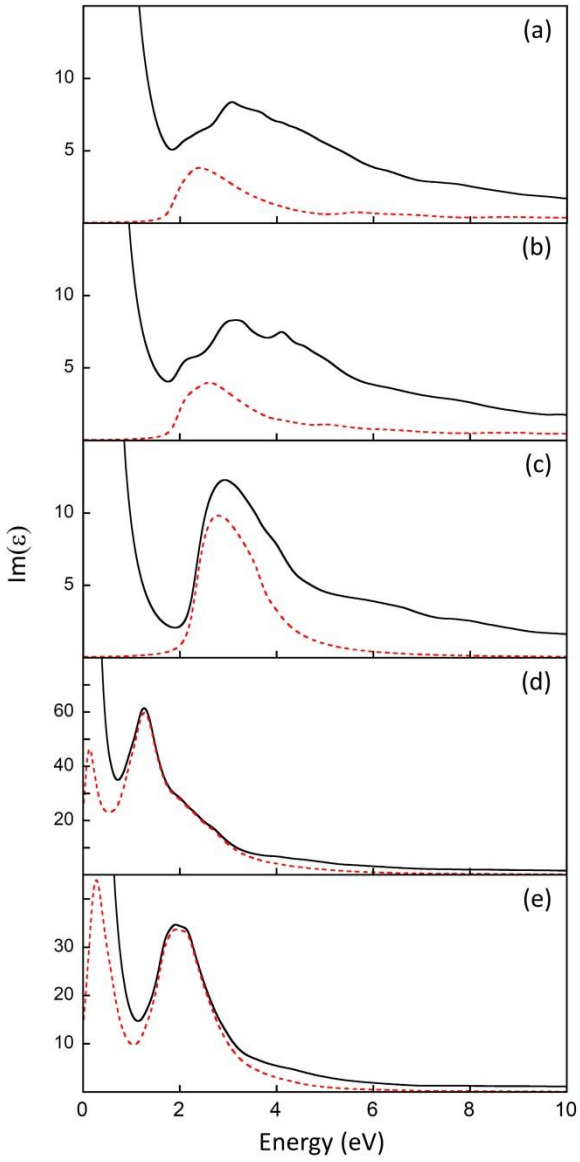

FIG 6

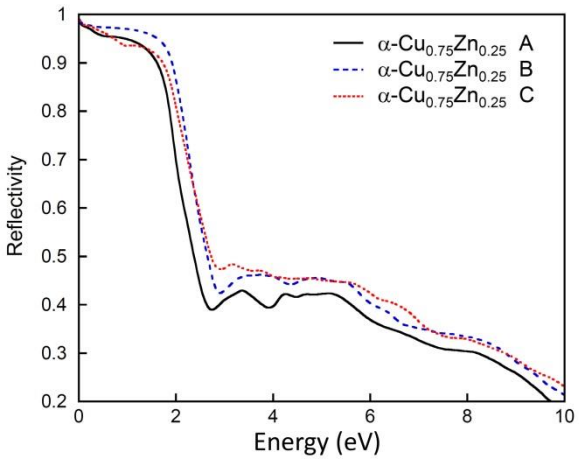
α-Cu0.75Zn0.25 A
α-Cu0.75Zn0.25 B
α-Cu0.75Zn0.25 C
Reflectivity
Energy (eV)
1
0.9
0.8
0.7
0.6
0.5
0.4
0.3
0.2
0
2
4
6
8
10

FIG 7

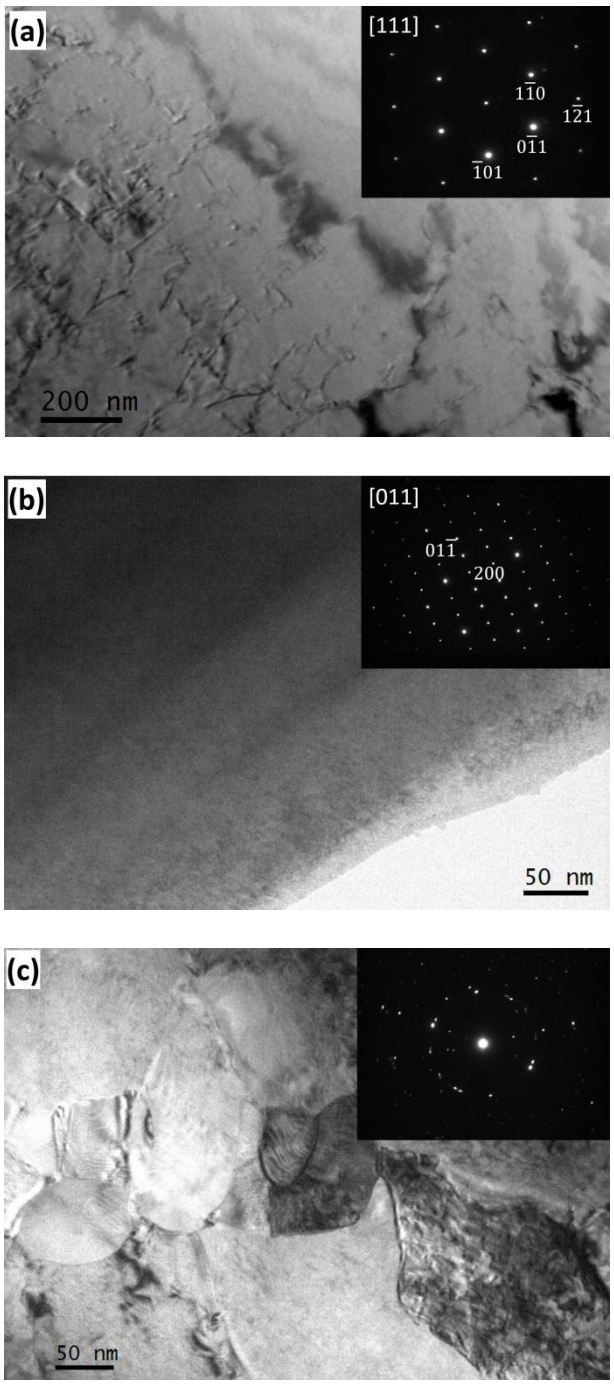
(a)
[111]
$1\bar{1}0$
$1\bar{2}1$
$0\bar{1}1$
$\bar{1}01$
200 nm
(b)
[011]
$01\bar{1}$
200
50 nm
(c)
50 nm